A DC to Multigigabit/s Polarization-Independent Modulator Based on a Sagnac Interferometer

Xiaojun Fang, *Senior Member, IEEE,* Helin Ji, Lawrence J. Pelz, *Member, IEEE,* Kenneth R. Demarest, *Member, IEEE,* and Christopher Allen, *Senior Member, IEEE*

***Abstract*— A broadband, electrically controlled polarization-independent intensity modulator (PIM) based on a Sagnac interferometer is presented. Influences from asymmetric modulation and traveling wave effects are analyzed and methods to eliminate these effects are proposed. Compared to Mach–Zehnder interferometer-based modulators, this modulator is independent of the input polarization state and less sensitive to ambient perturbations due to its reciprocity property. A prototype modulator operating at 1 and 2.488 Gb/s modulation rates is demonstrated.**

***Index Terms*—Birefringence, optical fiber devices, optical fiber polarization, optical modulation/demodulation.**

I. Introduction

HIGH-SPEED intensity modulators and switches are important components for optical fiber telecommunications. Current modulators include lithium-niobate-based Mach–Zehnder (M–Z) modulators [1], [2] and electroabsorption modulators [3], [4]. Optically controlled optical time-division demultiplexers based on optical nonlinearities [5], [6] may also be used for intensity modulation and switching, but the requirements of high optical power and synchronization makes them far from practical for commercial systems. Therefore, an electrically controlled optical scheme is currently the most practical method to attain lightwave modulation and switching because of the available microwave technology and reliability.

The two most popular intensity modulators, the M–Z modulator and the electroabsorption modulator, each have their own advantages and disadvantages. The M–Z modulator (MZM) has superior optical bandwidth and temperature stability compared to the electroabsorption modulator, but the input light's polarization state must be aligned along a principal axis of the device. On the other hand, the electroabsorption modulator (EAM) has less polarization dependence, but has higher insertion loss and narrower optical bandwidth. For applications such as high-speed photonic switching at a remote node in a network, the requirement of achieving a linearly polarized input is difficult to satisfy. Even on the transmitter side, polarization scrambling or depolarizing is usually required after an M–Z modulator to eliminate polarization hole burning in fiber amplifiers [7]. A polarization-independent modulator (PIM) could directly modulate an unpolarized input.

The only available electrooptic effect that offers ultrahigh response speed and reasonable drive voltage is the Pockels effect, which provides a method to control optical signals electrically. Commercial MZM's based on this effect can reach speeds up to 20 GHz. However, since the Pockels effect is an electric field-induced birefringence, the input polarization has to be aligned to the direction of the TE mode in the modulator. This requirement makes the MZM depend on input polarization orientation. The Sagnac interferometer-based modulator described in this paper displays the desirable property of polarization insensitivity. The organization of this paper is as follows. The principle of operation of this device will be discussed in Section II, and influences from traveling wave effects and asymmetric modulation will be addressed in Section III. A prototype polarization-independent modulator was tested and experimental results are given in Section IV.

II. Principle

The structure of the proposed polarization-independent modulator (PIM) is shown in Fig. 1. Here the fiber coupler is a low-loss 3 dB coupler, and the birefringence modulator is a lithium-niobate phase modulator based on the Pockels effect. Light is input to port 1 and output from port 2. The general form of Jones matrix representing the birefringence of the Sagnac loop and the electric field of input light are given by

$$M = \begin{bmatrix} A & -B^* \\ B & A^* \end{bmatrix} \tag{1}$$

and

$$E_{\text{in}} = \begin{bmatrix} E_x \\ E_y \end{bmatrix} \tag{2}$$

respectively. The output field at port 2 is given by [8]

$$E_{\text{out}} = i\,\text{Im}(B) \begin{bmatrix} E_y \\ E_x \end{bmatrix} \tag{3}$$

where $\text{Im}(B)$ represents the imaginary part of B. It is important to note from (2) and (3) that the amplitude transfer function of the electric field is independent of the input polarization state. The intensity transfer function of this device is given by

$$T = (\text{Im}(B))^2. \tag{4}$$

Manuscript received May 12, 1997.

X. Fang, H. Ji, K. R. Demarest, and C. Allen are with the Information and Telecommunication Technology Center, Department of Electrical Engineering and Computer Science, University of Kansas, Lawrence, KS 66045 USA.

L. J. Pelz is with Sprint, Overland Park, KS 66212 USA.

Publisher Item Identifier S 0733-8724(97)08128-0.

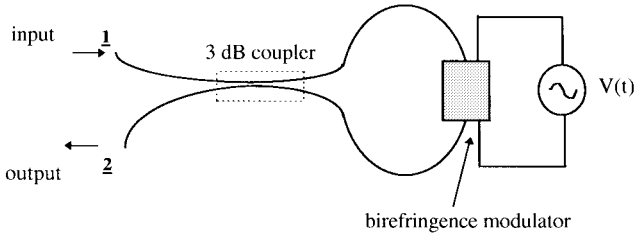

Fig. 1 Structure of a Sagnac interferometer-based PIM.

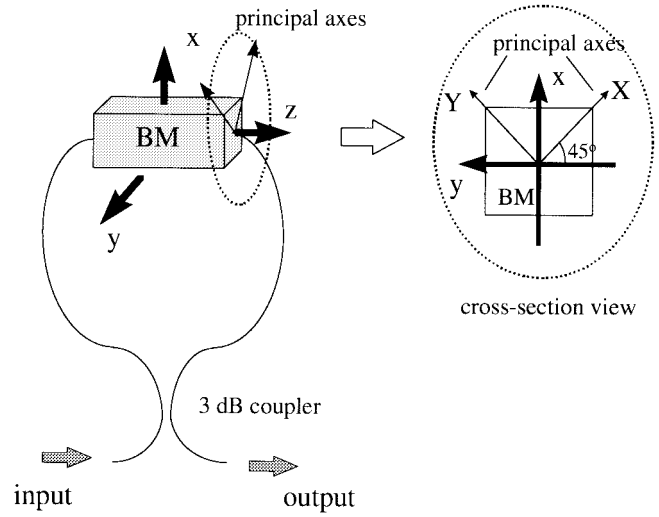

Fig. 2. Orientation of the principal axes of the birefringence modulator.

If we assume zero birefringence in the lead fibers, then the loop birefringence is contributed solely by the birefringence modulator. We will define the plane where the Sagnac loop lies as the x-z plane, and the light propagation direction as the z-axis. The cross section of the birefringence modulator is within the x-y plane and the principal axes of the birefringence modulator (X and Y) are along a 45° direction relative to the x and y axes. The orientation of this coordinate system is illustrated in Fig. 2 where, for clarity, the orientation of the principal axes of the birefringence modulator are illustrated in the enlarged area on the right. If the phase retardation of the birefringence modulator between the two orthogonally polarized modes is ϕ, then the Jones matrix of this modulator in this coordinate system is

$$M = \begin{bmatrix} \cos(\phi/2) & -j\sin(\phi/2) \\ -j\sin(\phi/2) & \cos(\phi/2) \end{bmatrix}. \tag{5}$$

Then, according to (4), the intensity transfer function of this device is given by

$$T = \sin^2(\phi/2). \tag{6}$$

If the phase retardation ϕ is modulated, the intensity transfer function will also be modulated accordingly. Assume ϕ is modulated by a sinusoidal signal

$$\phi(t) = \phi_0 + \frac{\pi}{2}\sin(\omega_m t) \tag{7}$$

where ϕ_0 is the initial phase retardation and ω_m is the modulation frequency. The change of the transfer function

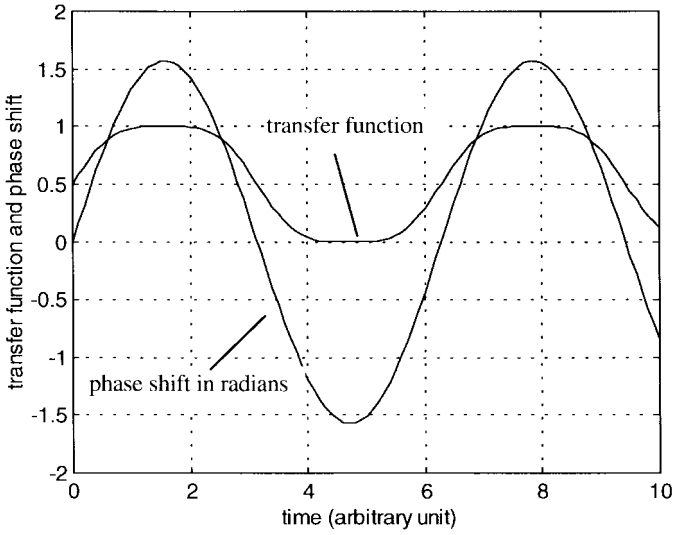

Fig. 3. Change of intensity transfer function and signal phase when a sinusoidal modulation is applied.

T together with the phase shift $\phi - \phi_0$ are shown in Fig. 3 where ϕ_0 determines the biasing point and is assumed to be $2N\phi + \phi/2$ with N being an integer. It can be seen from Fig. 3 that the dependence of the intensity transfer function for a sinusoidal drive voltage is similar to that of an M–Z modulator. Since the transfer function is flat at both the top and bottom positions, noise can be suppressed by the nonlinearity of the device. One point to note is that all components within this device are lossless, so the sum of the transmitted power and the reflected power will be equal to the total input power.

III. Influences from Traveling Wave and Asymmetric Modulation Effects

The intensity transfer function above is derived under the lumped condition where the wavelength of the modulation is much larger than the length of the Sagnac loop. As the frequency increases, traveling wave effects need to be considered. Also, if the phase modulation is not symmetric within the loop, pseudo-nonreciprocal phase shifts will be generated at the output of the Sagnac interferometer [9]. We will analyze these two influences separately and discuss ways to minimize them.

A. Traveling Wave Effect

When the modulation frequency is high (above 1 GHz), the lumped model for the birefringence modulator will not be valid. If the active path length of the modulator is l, the time it takes for light to pass through the active region of the modulator is given by

$$\tau = \frac{nl}{c} \tag{8}$$

where n is the refractive index of the optical waveguide and c is the velocity of light in vacuum. The transmission velocity of the RF signal is usually designed to match the velocity of the light, so that they transit through the modulator with the same speed. If we assume the modulation signal is sinusoidal, then

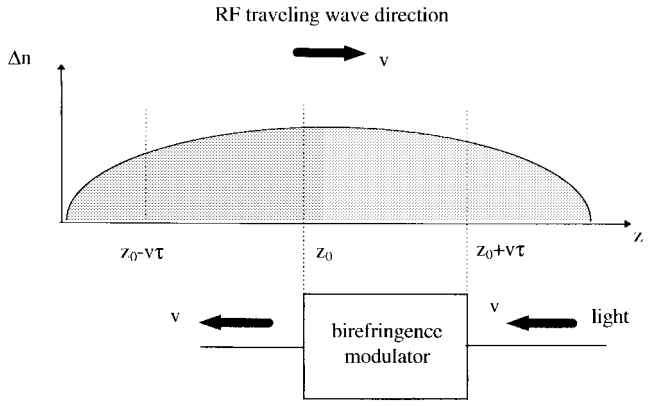

Fig. 4. Indication of the traveling wave effect for the reverse transmitting light. The birefringence in the birefringence modulator is a distributed parameter.

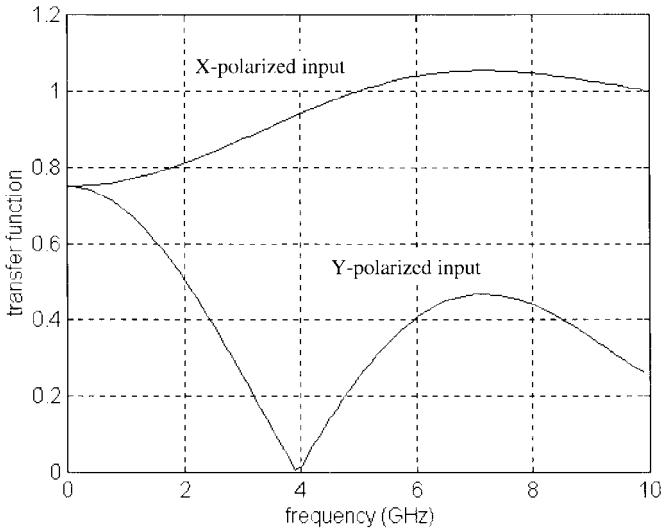

Fig. 5. Frequency response of phase signal for X-polarized and Y-polarized input.

the phase modulation of the light induced by the RF signal within the phase modulator is given by

$$\varphi_{\mathrm{CW}} = \frac{2\pi\Delta n l}{\lambda} = \varphi_0 \cos(\omega_m t) \tag{9}$$

where φ_0 is the amplitude of the phase modulation, Δn is the change of the refractive index induced by the modulation signal, and ω_m is the frequency of modulation. For reverse propagating light, the light travels opposite to the direction of the RF signal. Fig. 4 illustrates this process, where the traveling RF signal propagates along the z-axis and induces a distributed refractive index change Δn inside the phase modulator. It is not difficult to see that the phase modulation experienced by the reverse propagating light is an averaged version of the distributed phase shift signal over a time slot of 2τ. For this reason, the phase modulation of the reverse light signal can be written as

$$\begin{aligned}\varphi_{\mathrm{CCW}} &= \frac{2\pi\Delta\overline{n}(z)l}{\lambda} = \frac{1}{2\tau}\int_{t-\tau}^{t+\tau} \varphi_0 \cos(\omega_m t')\, dt' \\ &= \varphi_0 Sa(\omega_m\tau)\cos(\omega_m t)\end{aligned} \tag{10}$$

where φ_0 is the amplitude of the phase modulation as in (9), and $Sa(x)$ is a sample function defined as $\sin(x)/x$. By comparing (9) and (10), it is easy to see that there is a sensitivity reduction for the reverse propagating light. When $\omega_0\tau \ll 1$, the two equations are identical and the lumped circuit model is valid.

Next, we include the birefringence effect into the traveling wave consideration. For a lithium-niobate-based phase modulator, the change of refractive index for a TM mode is only about 1/4 of that for a TE mode [10]. The phase retardation between the counterpropagating waves used to derive (6) will in general depend on the input polarization state and be given by

$$\phi_X = \varphi_0[1 - \tfrac{1}{4}Sa(\omega_m\tau)]\cos(\omega_m t) \tag{11a}$$

$$\phi_Y = \varphi_0[\tfrac{1}{4} - Sa(\omega_m\tau)]\cos(\omega_m t) \tag{11b}$$

where ϕ_X and ϕ_Y are the phase differences of the counterpropagating signals for linear polarized inputs along the X–Y axes of the modulator, respectively. Since the intensity transfer function of the modulator is an even function of ϕ as shown in (6), this device will be polarization insensitive as long as $\omega_0\tau \ll 1$ is satisfied. But in the high frequency region, ϕ_X will not be the same as ϕ_Y, and the modulator will become polarization dependent. Higher frequency components of digital signals will have a higher polarization sensitivity than the lower frequency components. The transfer functions for the phase difference for an X-polarized and a Y-polarized input described by (11) are plotted in Fig. 5, assuming the transit time through the birefringence modulator is 100 ps.

The polarization dependence of the output signal can be more easily seen by examining the eye diagram of the output. A 1 Gb/s random bit sequence is used to simulate the output eye diagram for the two different input polarization states. The result is shown in Fig. 6 where we can see a smoothing effect due to the filter characteristic shown in Fig. 5. Note that the eye height remains the same and little power penalty will be contributed into a system from input polarization fluctuations. However, this is not true for higher modulation frequencies (10 Gb/s), where a large power penalty will be induced by the input polarization fluctuations.

In order to solve this problem, a balanced phase modulator structure is proposed and shown in Fig. 7(a). The principal axes of the two birefringence modulators are arranged parallel to each other as shown in the figure. Similar to (11), the phase shift in this balanced structure can be given by

$$\varphi_{\mathrm{CCW}} = \varphi_{\mathrm{CW}} = \varphi_0[\cos(\omega_m t) + Sa(\omega_m\tau)\cos(\omega_m t + \tau)]. \tag{12}$$

Thus, phase difference induced by the balanced birefringence modulator will be given by

$$\phi_X = -\phi_Y = \tfrac{3}{4}\varphi_0[\cos(\omega_0 t) + Sa(\omega_0\tau)\cos(\omega_0 t + \tau)]. \tag{13}$$

This result shows that the phase modulation is symmetric for the counterpropagating waves, and the traveling wave effect can thus be balanced. An ultrahigh-speed polarization-independent modulator can be achieved in this way.

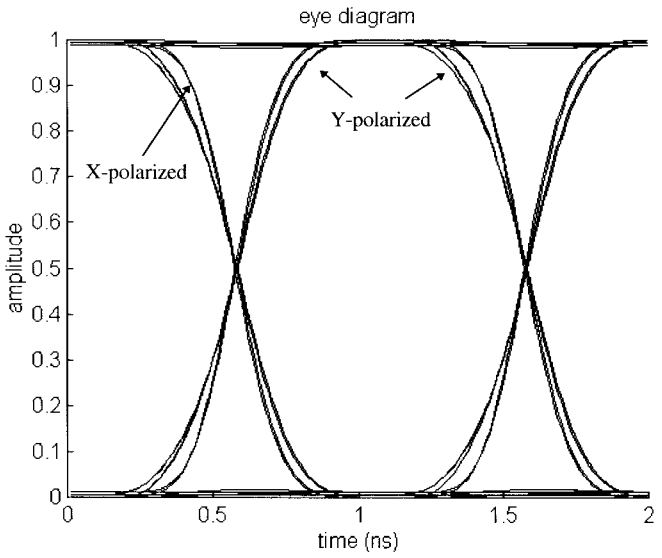

Fig. 6. Output eye diagram of the 1 Gb/s bit rate signal for X-polarized and Y-polarized input.

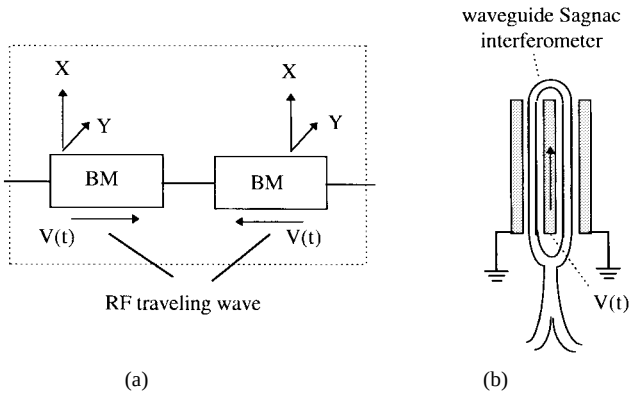

(a) (b)

Fig. 7. Structure of the proposed balanced birefringence modulator (a) and the PIM (b).

B. Asymmetric Modulation

If the birefringence modulator is not placed exactly in the center of the Sagnac loop, the asymmetric modulation will induce signal degradation. If we assume the birefringence modulator has been placed a distance x meters away from the center of the loop, as shown in Fig. 8, the orientation of the principal axes of the birefringence modulator is oriented in the same way as shown in Fig. 2. Because the birefringence of the modulator is time varying, its Jones matrix is time varying also. A lumped system model will be used for the birefringence modulator in this discussion.

Assume the length of the Sagnac loop is $2L$, the phase retardation of the birefringence modulator is $\phi(t)$, and the velocity of light inside the loop is V. The Jones matrix of the birefringence modulator becomes

$$M(t) = \begin{bmatrix} \cos[\phi(t)/2] & -j\sin[\phi(t)/2] \\ -j\sin[\phi(t)/2] & \cos[\phi(t)/2] \end{bmatrix}. \quad (14)$$

From Fig. 8, it is clear that the phase modulation experienced by the clockwise propagating light will lag the phase modulation experienced by the counterclockwise propagating

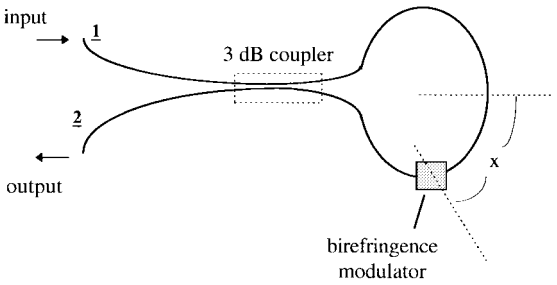

Fig. 8. An asymmetrically located birefringence modulator which is x meters away from the center of the Sagnac interferometer.

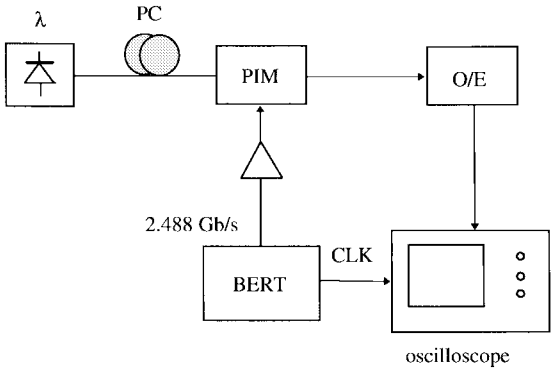

Fig. 9. Experiment setup to measure the high frequency polarization dependence of the PIM.

light. This lag is given by

$$\Delta t = \frac{L+x}{V} - \frac{L-x}{V} = \frac{2x}{V}. \quad (15)$$

By using the reciprocal condition [8], the Jones matrices for the clockwise-propagating light and counterclockwise-propagating light are given by

$$M_{\mathrm{CW}}(t) = \begin{bmatrix} \cos[\phi(t)/2] & -j\sin[\phi(t)/2] \\ -j\sin[\phi(t)/2] & \cos[\phi(t)/2] \end{bmatrix} e^{j\Omega(t)} \quad (16a)$$

and

$$M_{\mathrm{CCW}}(t) = \begin{bmatrix} \cos[\phi(t+\Delta t)/2] & j\sin[\phi(t+\Delta t)/2] \\ j\sin[\phi(t+\Delta t)/2] & \cos[\phi(t+\Delta t)/2] \end{bmatrix} Sa(\omega_m \tau) \quad (16b)$$

where Δt is given in (15). In general, the Sagnac interferometer-based modulator will be polarization dependent if the modulation is asymmetric. However, when the phase modulator is at the center of the loop $(x = 0), \Delta t = 0$, the intensity transfer function will return to the ideal form in (6) if the traveling wave effect is neglected. The influence of asymmetric birefringence modulation can thus be minimized.

IV. Experiment

To demonstrate the feasibility and to validate the polarization independence of the Sagnac interferometer-based ultra-high speed polarization-independent modulator, a dc to 2.488 Gb/s PIM was built with a 3 GHz lithium-niobate phase modulator. This modulator was placed in the middle of a Sagnac loop and connected with a polarization insensitive

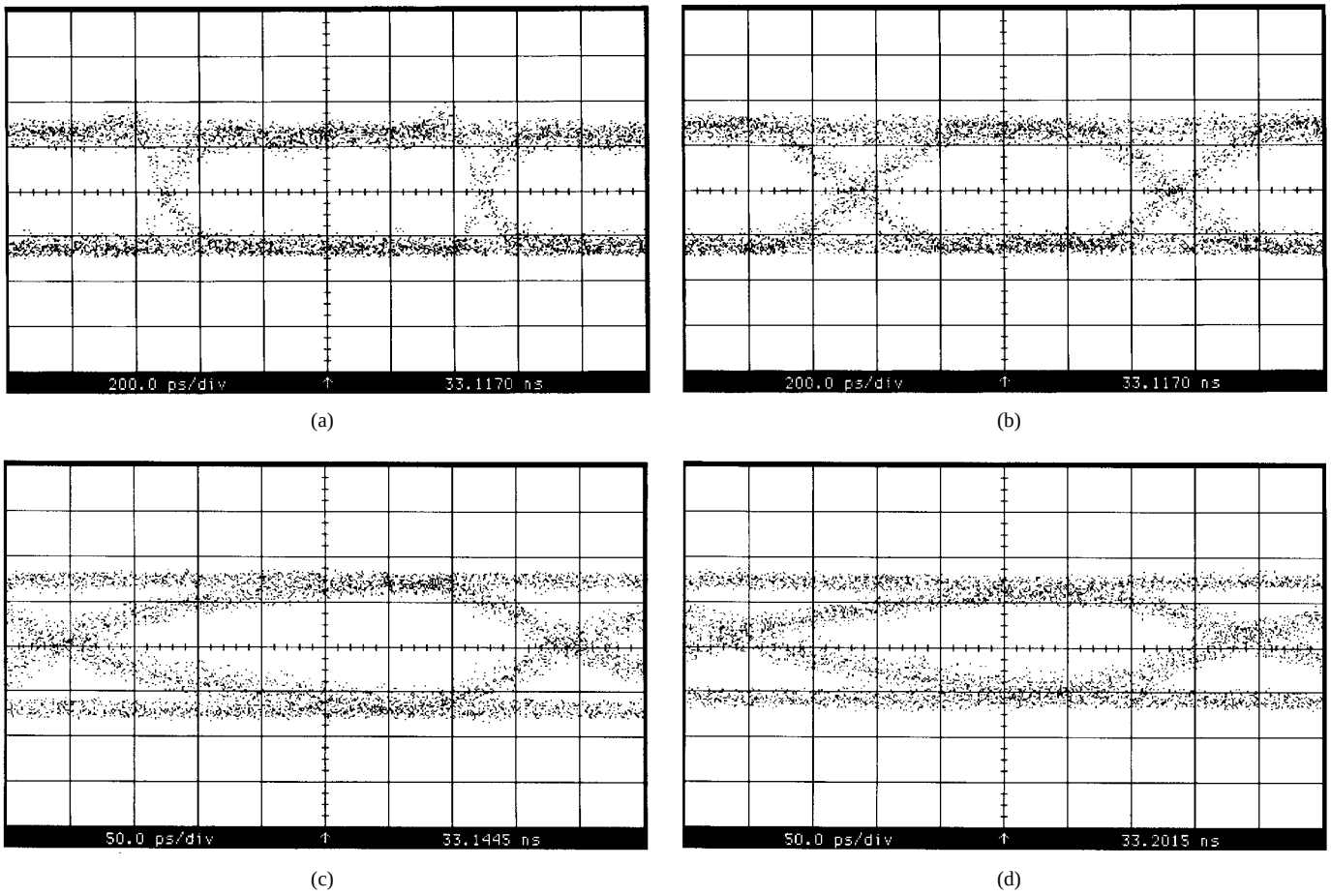

Fig. 10. Eye diagrams of the PIM output under different input conditions. (a) 1 Gb/s X-polarized input, (b) 1 Gb/s Y-polarized input, (c) 2.488 Gb/s X-polarized input, and (d) 2.488 Gb/s Y-polarized input.

3 dB fiber coupler to form a Sagnac interferometer. The experiment setup is shown in Fig. 9. A cw light signal from a 1550 nm DFB laser was injected into the PIM through a polarization controller (PC), and the PIM was driven by the pattern generator of an HP 71612A bit error rate tester (BERT). The output signal from the PIM was detected by a 6 GHz O/E converter and sent to a digital oscilloscope to measure the eye diagram of the output signal. The input state of polarization was controlled by adjusting the polarization controller.

The influence of the input polarization state on the output was examined by adjusting the polarization controller. Two bit rates of a $2^7 - 1$ pseudo-random bit sequence (PRBS) were used in the test and the eye diagrams with the widest eye width and narrowest eye width were recorded on the oscilloscope. Fig. 10(a) and (b) show the output eye diagrams for the 1 Gb/s signal. The filtering effect is clearly observed by comparing these two figures. This phenomenon agrees with the prediction as shown in Fig. 6. A bit rate of 2.488 Gb/s PRBS was also used and the eye diagrams are shown in Fig. 10(c) and (d). Because the 3 dB bandwidth of this particular birefringence modulator is only 3 GHz, the waveform is distorted and asymmetric. However the polarization dependence can still be identified by comparing the two figures. The sharp edges are smoothed out again for the Y-polarized input.

The property of the PIM under low modulation frequency was also tested. We used an optical power meter to monitor the output power and a dc voltage source to provide drive voltage. The extinction ratio and half-wave voltage V_π of the PIM were measured to be approximately 23 dB and 3 V, respectively, for a dc signal. For higher frequencies, V_π should increase considerably and reach 8 V for a 2 GHz signal. The drive voltage can be reduced by using the balanced structure shown in Fig. 7.

V. Conclusion

A broadband polarization-independent modulator (PIM) is described and test results have been presented. The main advantage of this device is that it utilizes the high-speed Pockels effect while keeping the device polarization independent. The employment of the Sagnac interferometer not only eliminates the input polarization dependence seen in a Mach–Zehnder modulator, but it also makes the biasing point of the device more stable to ambient perturbations. Liquid crystals, devices relying on the photoelastic effect or Faraday effect, could also be employed in this structure to build low-cost PIM's. In this way, polarization independent, broadband, stable photonic modulators can be realized.

References

[1] R. Marz, *Integrated Optics: Design and Modeling*. Norwood, MA: Artech House, 1995.
[2] R. Madabhushi, "Wide-band Ti:LiNbO3 optical modulator with low driving voltage," in *Tech. Dig. OFC'96*, 1996, p. 206.

[3] T. Ido, S. Tanaka, M. Suzuki, M. Koizumi, H. Sano, and H. Inoue, "Ultra-high-speed multiple-quantum-well electro-absorption optical modulators with integrated waveguides," *J. Lightwave Technol.*, vol. 14, p. 2026, 1996.
[4] C. Rolland, G. Mak, W. Bardyszewski, and D. Yevick, "Improved extinction ratio of waveguide electroabsorption optical modulators induced by an InGaAs absorbing layer," *J. Lightwave Technol.*, vol. 10, p. 1907, 1992.
[5] H. Avramopoulos, P. M. W. French, M. C. Gabriel, H. H. Houh, N. A. Whitaker, Jr., and T. Morse, "Complete switching in a three-terminal Sagnac switch," *IEEE Photon. Technol. Lett.*, vol. 3, p. 235, 1991.
[6] J. P. Sokoloff, I. Glesk, P. R. Prucnal, and R. K. Boncek, "Performance of a 50 Gbit/s optical time domain multiplexed system using a terahertz optical asymmetric demultiplexer," *IEEE Photon. Technol. Lett.*, vol. 6, p. 98, 1994.
[7] N. S. Bergano, C. R. Davidson, "Wavelength division multiplexing in long-haul transmission systems," *J. Lightwave Technol.*, vol. 14, p. 1299, 1994.
[8] X. Fang, R.O. Claus, "Polarization-independent all-fiber wavelength division multiplexer based on a Sagnac interferometer," *Opt. Lett.*, vol. 20, p. 2146, 1995.
[9] X. Fang, "A variable-loop Sagnac interferometer for distributed impact sensing," *J. Lightwave Technol.*, vol. 14, p. 2250, 1996.
[10] S. L. Chuang, *Physics of Optoelectronic Devices*. New York: Wiley, 1995.

Xiaojun Fang (S'94–SM'96) received the B.S. and M.S. degrees in electrooptic engineering from Dalian University of Technology, in 1985 and 1988, respectively, and the M.S. and Ph.D. degree in electrical engineering from Virginia Polytechnic and State University, Blacksburg, in 1994 and 1996, respectively.

He worked as a faculty member on fiber optic sensors and fiber optic remote monitoring systems during 1988 to 1992, and on fiber components and fiber communication theory during 1993 to 1996. After graduation from Virginia Polytechnic, he joined the Information and Telecommunication Technology Center at the University of Kansas, Lawrence, as a Research Engineer and worked on long-haul transmission impairments in DWDM systems, high-speed polarization-independent filters and switches, and high-speed solitons. He joined Sprint's Advanced Technology Laboratories, CA, as a Senior Applied R&D Engineer in 1997 and is currently working on the DARPA-sponsored National Transparent Optical Network (NTON), optical cross-connect, photonic layer architecture, state-of-the-art DWDM system testing, and evolving transmission and routing technologies.

Helin Ji (M'96) received the B.S. and M.S. in physics from Nanjing University, Nanjing, China, in 1989 and 1991, respectively. He received the M.S. degree in electrical engineering from the University of Kansas, Lawrence, in 1997.

From 1991 to 1994, he worked on high-temperature superconductors as a Research Assistant at the Department of Physics, Nanjing University. From 1996 to 1997, he worked in the Information and Telecommunication Technology Center at the University of Kansas, where his work centered on the generation and propagation of solitons on optical fibers. In 1997, he joined WorldCom as a Researcher and Development Engineer of optical transmission and networks.

He is a member of Sigma Pi Sigma and the American Physical Society.

Lawrence J. Pelz (S'92–M'95) received the B.S. degree in physics and the M.S. degree in electrooptics from the University of Dayton, Dayton, OH, in 1986 and 1989, respectively. He received the M.S. and Ph.D. degrees in electrical engineering from The Ohio State University, Columbus, in 1996.

From 1996 to 1997, he was a Member of the Technical Staff with Sprint's Technology, Planning and Integration group, where he directed research in emerging optical communication technologies. In his current position with Siemens Telecom Networks, he is developing ultrahigh-capacity optical transport products.

Kenneth R. Demarest (S'78-M'79) was born in Hackensack, NJ, on December 16, 1952. He received the B.S. degree in electrical engineering from John Brown University, Siloam Springs, AR, in 1974, and the M.S. and Ph.D. degrees in electrical engineering from The Ohio State University, Columbus, in 1976 and 1980, respectively.

From 1974 to 1979, he was a Graduate Research Associate with the ElectroScience Laboratory at The Ohio State University. From 1979 to 1984, he was an Assistant Professor in the Electrical Engineering Department of Lafayette College, Easton, PA. Since 1984, he has been with the Electrical Engineering and Computer Science Department at the University of Kansas, Lawrence, most recently as a Professor. His research interests are in the areas of fiber optic communications and electromagnetics. He is the author of a number of papers, book chapters, and the book *Engineering Electromagnetics* (Englewood Cliffs, NJ: Prentice Hall, 1998).

Dr. Demarest is a member of Eta Kappa Nu and the International Union of Radio Science, Commission B.

Christopher Allen (M'94–SM'95) received the B.S., M.S., and Ph.D. degrees in electrical engineering from the University of Kansas, Lawrence, in 1980, 1982, and 1984, respectively.

He joined the Electrical Engineering and Computer Science Department at The University of Kansas as an Assistant Professor in August 1994. Prior to joining the University of Kansas, he was with the AlliedSignal Kansas City Division where he was a Senior Staff Engineer and worked in the areas of high-speed digital design, radar systems analysis, and multichip module development. Preceding this, he was a Senior Member of the Technical Staff at Sandia National Laboratories, Albuquerque, NM, where he developed high-speed digital systems (including timing and control circuitry and direct digital waveform synthesis) for advanced radar systems, and he performed radar system design and analysis on a variety of programs.